New methods to improve the usability in Magnetic Resonance Frequency Microscopy

THESIS

submitted in partial fulfillment of the
requirements for the degree of

MASTER OF SCIENCE
in
PHYSICS

Author :	Martijn van Velzen, BsC
Student ID :	1046489
Supervisor :	MSc. M. de Wit
	Prof.dr.ir. T.H. Oosterkamp
2^{nd} corrector :	Prof.dr. J.M. van Ruitenbeek

Leiden, The Netherlands, January 22, 2018

New methods to improve the usability in Magnetic Resonance Frequency Microscopy

Martijn van Velzen, BsC

Huygens-Kamerlingh Onnes Laboratory, Leiden University
P.O. Box 9500, 2300 RA Leiden, The Netherlands

January 22, 2018

Abstract

While Magnetic Resonance Force Microscopy is capable of imaging three dimensional structures on nanoscopic scales, the number of practical applications so far has been limited, partly due to the complexity of the device. In this thesis we introduce the Easy MRFM, a way to increase the usability of MRFM. By seperating all MRFM components from the sample, we hope to remove some of the drawbacks of the previous Oosterkamp MRFM, allowing for easier data analysis and sample exchange. This thesis provides the theoretical calculations for the optimal set-up of the Easy MRFM and a preliminary proof of concept. Furthermore it describes a new way to analyse the measurements of the cantilever properties which would be better suited for the Easy MRFM. It also It includes the characterization of a new cantilever which could possibly be used inside the Easy MRFM to increase its sensitivity.

Contents

Chapter 1

Introduction

One of the current challenges in physics is to resolve the three dimensional structure of certain molecules like proteins. Current scanning probe techniques like Scanning Tunneling Microscopy (STM) and Atomic Force Microscopy (AFM) are only able to tell us something about the surfaces of involved samples. MRFM is a way to combine these techniques with the physics of Magnetic Resonance Imaging (MRI) to allow us to resolve three dimensional structures on a nanoscale. The first developments in MRFM came at the end of the 90's. In 2004 Rugar et al. were able to succesfully detect a single electron spin with a spatial resolution of 25 nm [1]. Probably the biggest accomplishment in MRFM so far has been the three dimensional imaging of the tobacco mosaic virus by Degen et al. in 2009 [2].

A lot of work has been done in our group to lower the operating temperature in the MRFM set-up. Unfortunately the implemented solutions caused an increased difficulty in handling the set-up. This thesis describes some of these difficulties and the work done to combat and solve them. Chapter three provides the theoretical foundation for a new set-up that is currently produced which would make MRFM easier to use. Chapter four goes into the way we process our data and describes the way a new program works that could be used to easily interpret results from our measurements. Chapter five explores the characteristics of new cantilevers that could possibly be used in our group.

Chapter 2

Theory

2.1 The mechanics of MRFM

Magnetic Resonance imaging (MRI) is currently one of the most well known and successful 3D imaging techniques around. The images are made by placing a sample inside a strong homogeneous magnetic field. The spins inside the sample are then perturbed through a radio-frequency (rf) magnetic field and their reaction is measured. One of the downsides of MRI is its low resolution limits. MRFM tries to overcome this low resolution limit by combining Magnetic Resonance with Probe Microscope technology.

Our own set-up has a resonating cantilever set above the surface of our sample. We use a micro sized magnetic particle on the tip of the cantilever to create a magnetic field in the order of 10^5 - 10^6 T/m [3]. Trough this field the cantilever is coupled with the spins in the sample.

By placing an rf wire on our sample, we can create rf pulses that can also manipulate the spins in the sample. Because of the strong field created by the magnetic particle, most of the spins in the sample will be unperturbed by the rf pulse. Only in a small slice in the sample called the resonance slice, the rf pulse will flip the spins. Since these spins are still coupled to the cantilever the perturbation will influence the motion of the cantilever.

This resonance slice is defined by the resonance condition $\omega_{rf} = \gamma B_0$ where ω_{rf} is the frequency of the rf pulse, γ is the gyromagnetic ratio of the sample and B_0 is the field created by the particle. By changing the frequency of the rf pulse, the resonance slice can be moved through the sample according to the gradient of the magnetic field. We can thus image the resonance slice of our sample by monitoring the motion of the cantilever and control where the resonance slice is in our sample through the

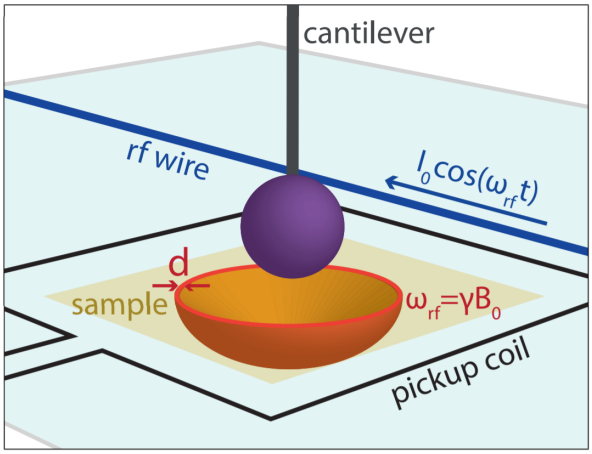

Figure 2.1: *A schematic of an MRFM measurement. The B1 field generated by sending a current through the RF wire manipulates the spins within the resonance slice, which is shown in orange. The alterned magnetization influences the cantilever and changes its properties, which can then be measured using the pick-up loop. [3]*

frequency of our rf pulse. By measuring multiple slices it is possible to create a three dimensional representation of our sample on the nanoscale.

The way we measure the perturbed motion of the cantilever is through its varying magnetic field. In current measurements a pick-up loop is placed on the surface of our sample. This pick-up loop is coupled to a Superconducting Quantum Interference Device (SQUID) which is able to measure changes in the magnetic field going through the pick-up loop. This all is done in a vacuum and temperatures of a few milikelvin to reduce noise and increase sensitivity.

2.2 Cantilevers

The most vital part in every MRFM set-up is the cantilever. It is the sensor in your measurements which is extremely sensitive to the perturbation in your sample. To understand the effect of these perturbations, the mechanics of a cantilever must be fully understood. In this section we will first explain the important parameters of a cantilever, the Q-factor and the resonance frequency. Then we will show how to model a cantilever and predict their resonance frequency. Furthermore we will show the current method to measure the quality factor and the resonance frequency of a cantilever through its transfer function.

2.2.1 Quality factor & Resonance frequency

The most important parameters of a cantilever are its resonance frequency and its Quality factor (Q-factor). In a MRFM measurement the cantilever oscillates because its driven by a small piezoelectric element. Its amplitude depends on the frequency of the piezo and the cantilevers own resonance condition. The resonance frequency of a cantilever is the frequency at which the cantilever oscillates with the highest amplitude.

The Q-factor is defined as 2π times the energy stored in the cantilever divided by the energy lost in one oscillation. A cantilever with a higher Q-factor thus loses less of the energy stored and retains its resonance longer after the driving force is removed. The Q-factor also characterizes the bandwidth relative to the resonance frequency, where a higher Q-factor means a better defined resonance frequency.

2.2.2 Calculating the resonance frequency

It is a lot easier to find the resonance frequency of your cantilever if you know where to look. Therefore it is important to be able to predict the resonance frequency of a cantilever. Below we explain multiple ways to predict the resonance frequency depending on the circumstances.

Continuous beam

It is possible to calculate the resonance frequency of a continuous beam through the formula [4]

$$\omega_0 = 2\pi * f_0 = \sqrt{\frac{k}{M_{eff}}} \tag{2.1}$$

Here k is the stiffness of the beam and is calculated by $k = \frac{E*W*T^3}{4*L^3}$ where E stands for Youngs modulus and is a property of the material used, W is the width of the beam, T is the thickness and L is the length of the beam. M_{eff} is the effective resonating mass, which for an unloaded continuous beam, equals $\frac{33}{140}$ times the total mass of the beam (M_{beam}) [5].

Loaded continuous beam

While normal cantilevers can be easily approximated as a continuous beam, we have no use of them unless they create a magnetic field. For this we place a tiny magnetized particle of a few micrometres on the tip of our

Version of January 22, 2018– Created January 22, 2018 - 16:50

cantilever. This particle changes the effective mass of the cantilever and thus changes its resonance frequency. With one particle on the end of the cantilever this is simply solved by adding the mass of the particle to the effective mass of the beam. $M_{eff} = M_{particle} + \frac{33}{140} * M_{beam}$.

In some instances it can be useful to put multiple particles on the cantilever. While the resonance frequency for this set-up could be calculated it is far easier to make an approximation. For every distinct particle we calculate the angular frequency of a cantilever where the other particles, and the part of the cantilever behind the particle, was removed. The length of this cantilever thus equals the distance of the particle on the original cantilever. We calculate the multiple angular frequencies with $\omega_i = \sqrt{\frac{k_i}{M_{eff,i}}}$. Our approximation for the angular frequency of the original cantilever is then given by Dunkerley's equation [6]:

$$\frac{1}{\omega^2} = \frac{1}{\omega_1^2} + \frac{1}{\omega_1^2} + ... + \frac{1}{\omega_n^2} \tag{2.2}$$

From which we can find our wanted resonance frequency by $f_0 = \frac{\omega}{2\pi}$. Dunkerley's equation is a lower bound to the exact solution where experimentation showed an error less than 5% although this is not guaranteed by the method [7].

We tested this method by calculating the resonance frequency of a 138.06 μm silicon cantilever with a thickness of 100 nm and a width of 5 μm. the cantilever has a particle of radius of 0.95 μm on the end of the cantilever and a particle of radius of 1.82 μm at 7.28 μm from the end. The estimated frequency using this method is 2961 Hz while experimentally we got a resonance frequency of 3075 Hz. Our estimate is thus in compliance with the theory as a lower bound with an error of 3.7%.

Comsol simulations

An easier but computational wise heavy simulation is achieved using the Comsol program. Comsol uses finite element analysis to calculate the behaviour of the specified geometry. By building a cantilever and specifying its boundary parameters we get a visual simulation of our cantilevers behaviour. Furthermore Comsol is also able to calculate the higher resonant modes than the fundamental one, which could be used as an rf source [8]. A cantilever can also be driven at its higher modes by a magnetic field, if they have the same frequency. This is something to avoid because it makes your signal harder to interpret. For real insight into a cantilevers

Version of January 22, 2018– Created January 22, 2018 - 16:50

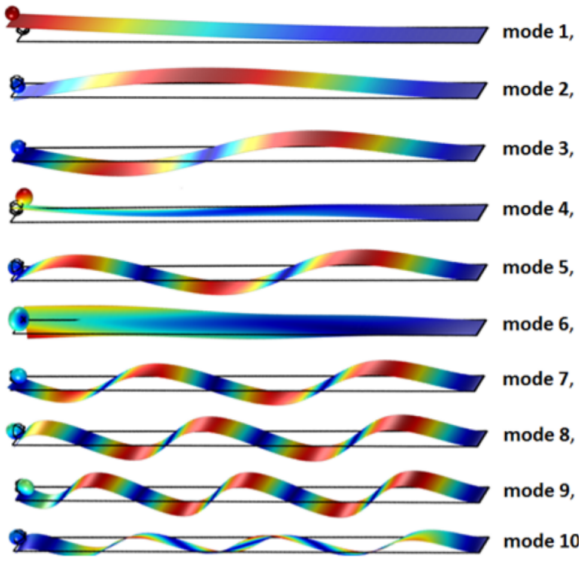

Figure 2.2: *A visualization of the multiple modes of a simulated cantilever in comsol. [9]*

behaviour it is thus useful to study Comsol simulations but for rough estimates it is a lot faster to use the above equations.

2.3 The transfer function

We need to know how a cantilever reacts to an external force to understand our gathered data. The differential equation for a driven cantilever is given by:

$$m_{eff}\ddot{x} = -k_0 x - \gamma\dot{x} + F_{drive}(t) \tag{2.3}$$

where m_{eff} is the effective mass of a cantilever, k_0 is the stiffness, x is the motion of the cantilever with the dots representing time derivatives, γ is the friction of the cantilever and $F_{drive}(t)$ is the driving force from the piezo. This equation is solved in the Fourier domain and gives us the following equation which we call the transfer function:

$$\frac{k_0 X(f)}{F_{drive}(f)} = \frac{1}{1 - \left(\frac{\omega}{\omega_0}\right)^2 + i\frac{\omega}{\omega_0 * Q}} \tag{2.4}$$

where again $w_0 = \sqrt{\frac{k_0}{m_{eff}}}$ and when we stay close to the resonance

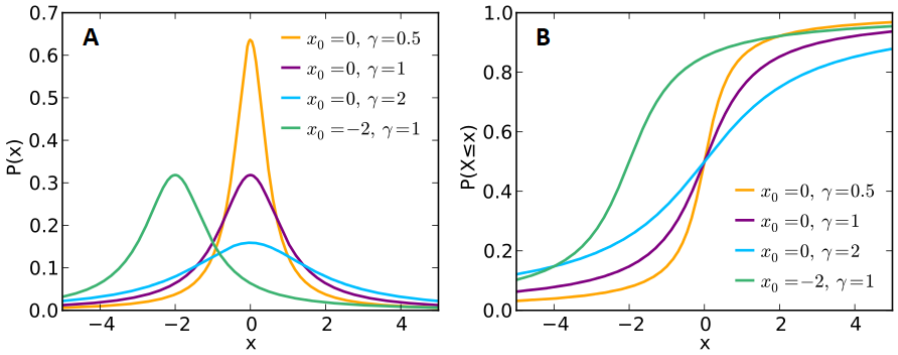

Figure 2.3: *A) A standard Lorentzian following* $f(x) = \frac{1}{\pi}\left[\frac{\gamma}{(x-x_0)^2+\gamma^2}\right]$*, showing the behaviour for different values of* γ *and* x_0*. B) The cumulative distrubition function of A. It is indicative of the phase measurements in MRFM experiments where the phase makes an 180 degree shift around the resonance frequency.*

frequency $\left(1 - \frac{\omega}{\omega_0} << 1\right)$ we can define the Q-factor as $Q = \frac{m_{eff} 2\pi f_0}{\gamma}$. If we square equation 2.4 and call the left sided part y(f) we get:

$$y(f) = \frac{2A}{\pi} \frac{B}{4(f - f_0)^2 + B^2} \tag{2.5}$$

The above is a Lorentzian function which we can use to fit our data. Here A and B are our fitting parameters where A = $\frac{Qf_0\pi}{2}$ and B = $\frac{F_0}{Q}$. It shows that the height and width of the peak are thus defined by the Q-factor. A larger Q-factor furthermore gives a larger A and smaller B, which respectively gives a bigger and more sharply defined peak. Figure 2.3 shows the shape and behaviour of a standard Lorentzian function.

In conclusion, this transfer function gives us the means to measure the resonance frequency and Q-factor. We do this by measuring the amplitude and phase of the cantilevers oscillation while driving the piezo in a range of frequencies that contains the resonance frequency. By squaring these amplitudes and fitting them with the Lorentzian Function we can directly calculate the resonance frequency and Q factor.

Chapter 3

Easy MRFM

In this chapter we will introduce the Easy MRFM, a way to increase the usability of MRFM. We will also show the theoretical work that has been done before the start of development. There are three important pieces that determine the sensitivity in MRFM: the sample, the cantilever and the pick-up loop. We will first explain how to calculate the coupling between the sample and the cantilever and then the coupling between the cantilever and the pick-up loop. When we know all the parameters that determine the coupling, we will combine them to predict the optimal set-up for the Easy MRFM. The eventual Easy MRFM is now in production with close collaboration from the company Delft Circuits [10].

3.1 Introducing the Easy MRFM

One of the big problems in our current MRFM set-up is finding the right positioning. When cooling the MRFM from room temperature to 10 mK, thermal contraction results in a shift of the position of the cantilever with respect to the position at room temperature. The biggest part of this shift can be predicted by calculating the thermal contraction for all individual components of the setup. However, especially after changes to the sample or cantilever, we can still end up with an uncertainty in the final position of tens of microns in every direction. Finding the real position of the cantilever can take days, and optimizing your location in reference to the pick-up loop, rf wire and your sample is difficult, which makes it currently uninteresting for possible practical applications. Other downsides of our current method are the limitation to samples that can hold a pick-up loop or samples that can be placed on a detection chip. Furthermore, replacing

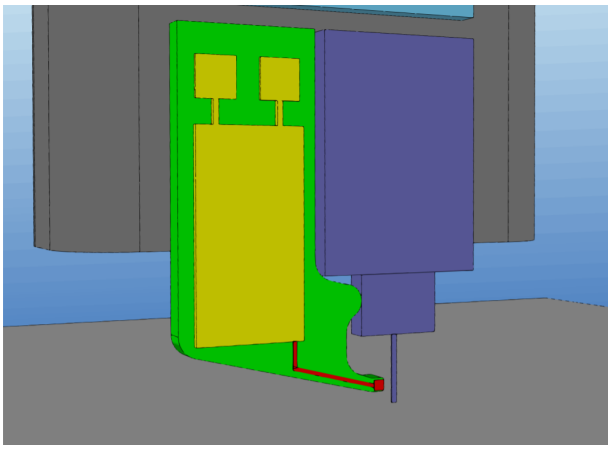

Figure 3.1: *One of the first design drafts of the Easy MRFM. On the left we see a green chip, containing the red pick-up loop and yellow electronics. The purple chip on the right contains the cantilever.*

the sample is at this moment a long process because the new sample also needs a new pick-up loop.

For these reasons, we propose a new MRFM setup where all components required for the MRFM experiment are seperated from the sample, as illustrated in figure 3.1. Here the pick-up loop is positioned beside the cantilever while recent measurements have found it possible to replace the rf wire using the higher modes of the cantilever [8]. This new approach would remove the dependence of the detection sensitivity on the position of the cantilever, and allow for quicker sample exchanges. We call this version the Easy MRFM.

3.2 Coupling Sample & cantilever

To get an estimate of the signal we should expect with the Easy MRFM, one of the things we need to know is the coupling between the sample and the cantilever. As an example, we want to calculate the frequency shift and change in quality factor of the cantilever when it is close to a sample, without applying magnetic resonance pulses. We calculate this using the formulas derived by Marc de Voogd [11].

$$\frac{\Delta f}{f_0} = \frac{1}{2} C \cdot \frac{(2\pi f_0 T_1)^2}{1 + (2\pi f_0 T_1)^2} \tag{3.1}$$

$$\Delta\frac{1}{Q} = C \cdot \frac{2\pi f_0 T_1}{1 + (2\pi f_0 T_1)^2} \tag{3.2}$$

$$C = \frac{\sigma\mu^2}{k_0 k_B T} \iint_S \frac{\left(\hat{\mathbf{B}}(\mathbf{r}) \cdot \frac{\partial \mathbf{B}(\mathbf{r})}{\partial x}\right)^2}{\cosh^2(\frac{\mu B(\mathbf{r})}{k_B T})} d\mathbf{r} \tag{3.3}$$

Where T is the temperature, k_0 the natural stiffness of the cantilever, k_B is the Boltzmann constand , T1 is the spin's longitudinal relaxation time, σ is the spin density which we assume is constant and μ is the magnetic moment originating from the localized electron spins.

For a given temperature, relaxation time, and spin density, we only have to calculate the value of the magnetic field at each spin location, $\mathbf{B}(\mathbf{r})$. This field is produced by the magnet at the end of the cantilever. Since our magnets are almost perfectly spherical, we can threat them as a magnetic dipole, whose field can be described by:

$$\mathbf{B}(\mathbf{r}) = \frac{\mu_0}{4\pi}\left(\frac{3\mathbf{r}(\mathbf{m}\cdot\mathbf{r})}{r^5} - \frac{\mathbf{m}}{r^3}\right) \tag{3.4}$$

This makes it clear that the real parameters for the coupling between the sample and the cantilever are the magnets dipole moment and the distance between the sample and the magnet.

3.2.1 Optimalisation

With the distance between the sample and the polarization of the magnet being the deciding parameters for the coupling it is important to know how to optimize them. Figure 3.2 shows the relative frequency shift with a varying distance between the cantilever and sample for three different polarizations. These predictions hold for a cantilever with a resonance frequency of 3000 Hz, a relaxation time of 0.39 ms, a temperature of 10 miliKelvin and a 3 μm radius (R_0) and 1.3 T remanent magnetization of the dipole where $|\mathbf{m}| = \frac{1}{3} * R_0^3 * RMT$. It clearly shows a higher relative frequency shift closer to the sample, which makes sense because of the behaviour of the magnetic field with $\frac{1}{r^3}$. Far from the sample the z-polarization gives the highest relative frequency shift. It is important to note that the z-polarization interacts with the least amount of spins through the geometry of its magnetic field. Close to the sample the y-polarizations gives a slightly higher frequency shift than the z-polarization and is roughly a factor of 1.5 bigger than the shift for the x-orientation.

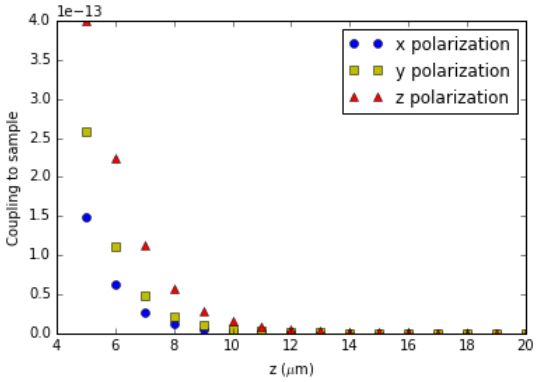

Figure 3.2: *We plotted the relative frequency shift for all three polarizations with a varying distance to the sample. It is clear that the relative frequency shift increases closer to the sample. Close to the samply the y-polarization gives the biggest relative frequency shift while the further away the z-polarization is bigger. The x-polarization continually gives the worst relative frequency shift but close to the sample the difference is only a factor 1.5*

Because the relative frequency shift is only dependent on C we can also extrapolate these results for the quality factor.

3.3 Coupling cantilever & pick-up loop

3.3.1 Location pick-up loop

Probably the most important determining factor of the feasibility of the Easy MRFM is the coupling between the cantilever and the pick-up loop. There are many ways to position the pick-up loop with respect to the cantilever. We feared that a snap to contact could occur when the pick up loop is positioned to close to the cantilever. Since this is most likely to happen along the soft direction of the cantilever, we have decided to place the pick up loop next to the stiffer axis of the cantilever like in figure 3.3.

Still, even in this positioning enough torsion on the cantilever could make it twist and clasp to the loop. This torsion could result from attractive forces (e.g. electrostatics) between the ultrasoft MRFM cantilevers, and the (relatively speaking) enormous detection chip, which will only be seperated by several micrometers. To calculate how much torsion is needed for this we can use the torsion formula:

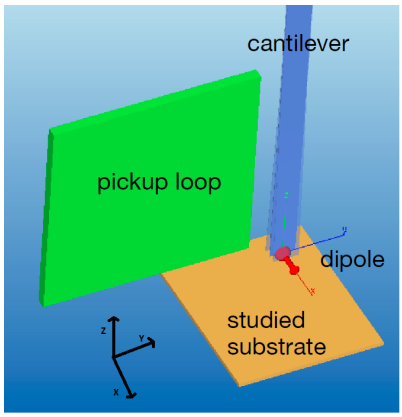

Figure 3.3: *Illustration of a possible Easy MRFM design with the pickup loop positioned parallel to the soft direction of the cantilever in the x-dimension. In this configuration, we prevent a snap to contact which would be a real possibility with the pickup loop crossing the cantilevers soft direction.*

$$T = \frac{\phi * G * J}{l} \tag{3.5}$$

Where ϕ is the angle of twist in radians, l is the length of the object and G is the Modulus of rigidity (shear modulus) of the material. J is the torsional constant which can be estimated for a rectangle with the formula

$$J = ab^3 \left(\frac{1}{3} - 0.21 \frac{b}{a} \left(1 - \frac{b^4}{12a^4} \right) \right) \tag{3.6}$$

where a is the length of the long side of the rectangle and b is the length of the short side and the result has a maximum error of 4% [12].

From the required torque to turn the cantilever towards the pick-up loop we can calculate the required force using the torque formula:

$$F = \frac{T}{r * \sin\theta} \tag{3.7}$$

With θ the angle between the force vector and the lever arm vector and r the position vector, a vector from the origin of the coordinate system defined to the point where the force is applied.

If we make the calculation for our new cantilevers described in Chapter 5, with the parameters described in table 3.1, it turns out we would need

Table 3.1: *Parameters of the new cantilevers*

ϕ	a	b	L	v	E	r	θ
$\frac{\pi}{2}$	1.0 μm	0.1 μm	130 μm	0.25	$210 * 10^9$	1 μm	$\frac{\pi}{2}$

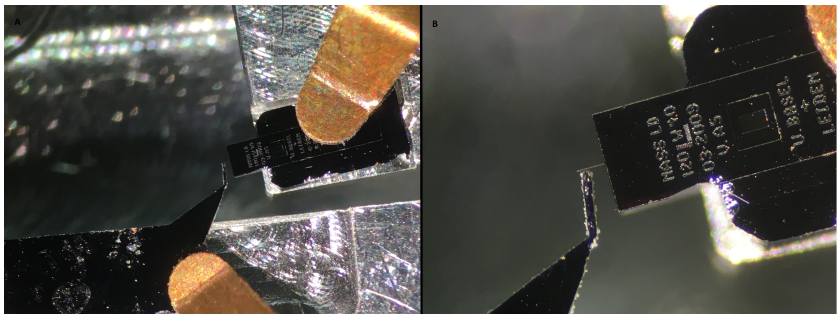

Figure 3.4: *The dummy sample placed besides the cantilever. With the dummy 11.8 μm from the sample it still shows no sign of bending towards it. This experimental test strengthens the conclusion of our calculation that snap to contact between the cantilever and the Easy-MRFM chip is unlikely.*

a force of at least 0.3 μNewton. It is not probable that effects like electrostatic forces would reach these strengths so this set-up should be safe for our cantilever. After we calculated that it was theoretically possible, we made some dummy samples to test it experimentally. These dummy samples are tiny chips on which we will eventually place a pick-up loop. Figure 3.4 shows the dummy 11.8 μm from the cantilever without bending to it. This proves that this set-up is possible and takes away one of the major concerns about the feasibility of the easy MRFM.

3.3.2 Coupling to pick-up loop

The magnetic field from our oscillating cantilever causes a changing flux through the pick-up loop, which in turn causes an varying electrical current $I = \Phi/L$. With I being the current, Φ the flux and L the inductance of the pick-up circuit. It is important to have the maximum coupling between the changing flux and the induced current so we can measure the tiniest changes in the resonance of the cantilever. We can model the coupling by calculating the derivative of the induced flux through the area of the pick-up loop. The flux through the pick-up loop can be calculated using formula 3.8.

Version of January 22, 2018– Created January 22, 2018 - 16:50

$$\Phi = \int_{pl} \overrightarrow{B} \cdot d\overrightarrow{a}_{pl} = \oint_{pl} \overrightarrow{A} \cdot d\overrightarrow{L}_{pl} \tag{3.8}$$

with $\overrightarrow{A}$ being the vector potential of a dipole moment which is calculated using (3.9)

$$\mathbf{A}(\mathbf{r}) = \frac{\mu_0}{4\pi}\left(\frac{\mathbf{m}\times\mathbf{r}}{r^3}\right) = \frac{\mu_0}{4\pi}\left(\frac{\mathbf{m}\times\mathbf{r}}{\sqrt[3/2]{x+y+z}}\right) \tag{3.9}$$

By taking the derivative of the flux to the soft direction of the cantilever, which in general is taken as the x dimension, we get the coupling. we also need to take into account the coupling of the pickup loop to the input coil of the SQUID. Due to a mismatch in the inductance of the different coils, roughly 1% of the flux induced in the pickup loop reaches the SQUID.

For this coupling the parameters we can control are thus the polarization + strength of the magnet but also the location + dimension of the pick-up loop. We have plotted the predicted coupling based on the positioning of the cantilever in reference to the pick-up loop. There are two possibilities, namely the pick-up loop perpendicular with the motion of the cantilever (as shown in figure 3.5), and the pick-up loop parallel to the motion of the cantilever (as shown in figure 3.6).

The three plots in both pictures show the magnitude of the coupling with the pick-up loop depending on the position of the cantilever. For the tip of the cantilever on the position (X, -10, Z) the magnitude of the coupling is shown on the y-axis in a logarithmic scale. The pick-up loop is a square with sides of 30 μm placed 10 μm away from the cantilever on the y axis.

While the coupling for the perpendicular set-up is continuously higher, the maximal difference in the coupling is only a factor 2. For manufacturing reasons we chose to place the pick-up loop parallel next to the cantilever in the easy MRFM. Figure 3.7 shows the predicted coupling for a parallel loop with a frontal view. It is important to note that for the X polarization it is vital not to align the cantilever directly with the pick-up loop cause this will result in an almost negligible coupling.

3.3.3 Sanity check

We want to know if the predictions of our simulation are trustworthy. Therefore we first did a sanity check with data from earlier experiments.

Version of January 22, 2018– Created January 22, 2018 - 16:50

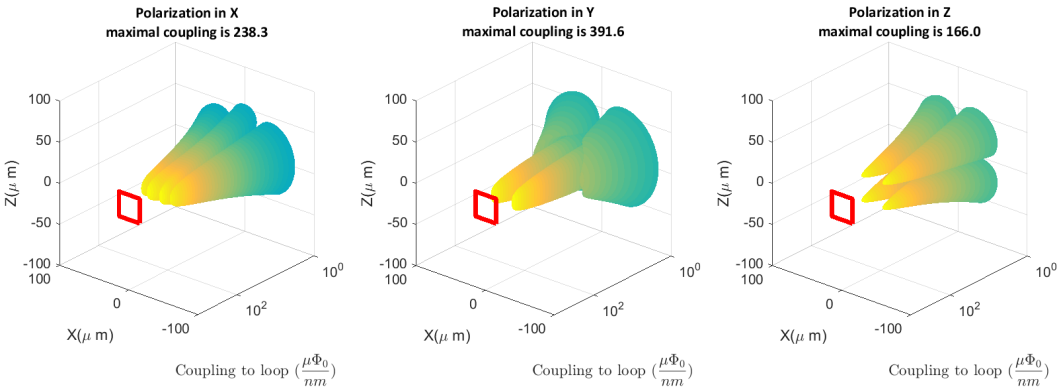

Figure 3.5: *The coupling with the pick-up loop perpendicular to the motion of the cantilever. The peak is the predicted coupling for a cantilever positioned at those x and z coordinates. The cantilever is at a constant 10 μm distance from the pick-up loop on the y-axis.*

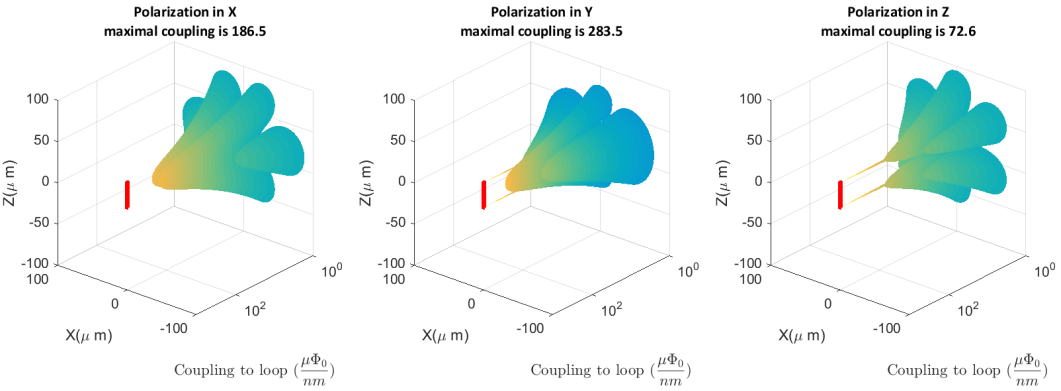

Figure 3.6: *The coupling for a parallel positioning. The pick-up loop is strangely displayed because of the logarithmic y-axis. The peak is the predicted coupling for a cantilever positioned at those x and z coordinates. The cantilever is at a constant 10 μm distance from the pick-up loop on the y-axis.*

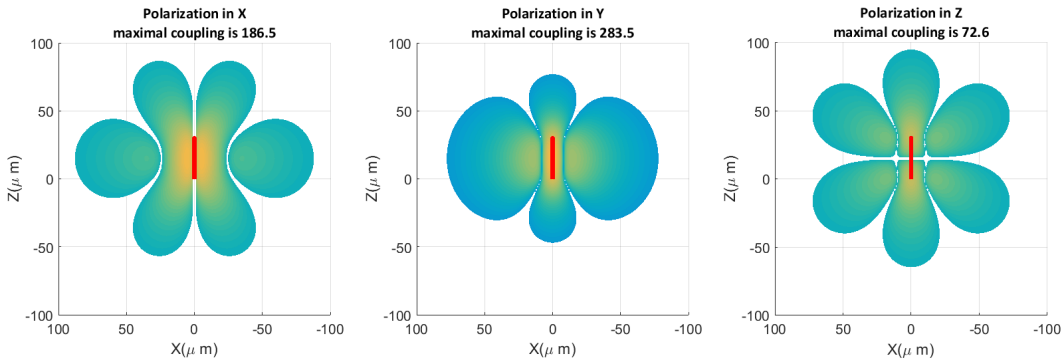

Figure 3.7: *A frontal view of the plot from figure 3.6 showing more clearly how the coupling depends on the positioning of the cantilever.*

In these experiments a 30*30 μm pickup-loop on the sample reached a detection sensitivity of 10 $pm/\sqrt{hz}$ with the cantilever roughly 20 μm above the sample [3] and the magnet polarized in the same direction as the movement of the cantilever. The detection sensitivity is the noise generated by the SQUID divided by the coupling which means that with a SQUID noise of 1 $\mu\Phi_0/\sqrt{hz}$ we should find a coupling of roughly:

$$Coupling = \frac{SQUID\ noise}{detection\ sensitivity} = \frac{1\ \mu\Phi_0/\sqrt{hz}}{10\ pm/\sqrt{hz}} = 10^2\ \mu\Phi_0/nm \quad (3.10)$$

Our predictions already take into account that only 1% of our signal reaches the measuring SQUID. In the same set-up as mentioned above our maximal simulated coupling is 75 $\mu\Phi_0/$ nm. This excellent agreement between the calculation and the experiment confirms the accuracy of our calculation, and increases our confidence in the predictions for the performance of the easy-MRFM.

3.4 Optimal set-up

With the placement of the pick-up loop decided based on the fabrication feasibility, we still need to determine the orientation of the magnet on the tip of the cantilever. We showed that for the coupling with the sample, the y-orientation was optimal, although is was only a factor 2 bigger than the x-orientation. Determining the optimal coupling to the pick-up loop is more difficult because it also depends on the positioning and dimensions of the loop. Current measurements are done with a square loop on the

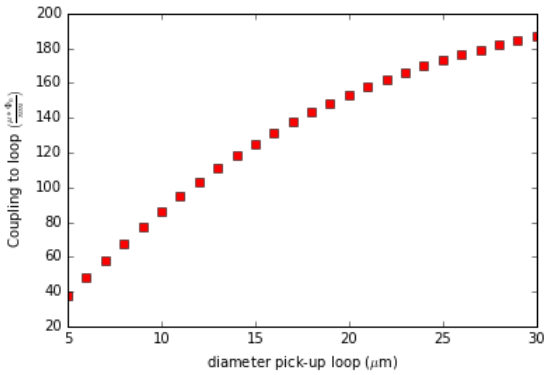

Figure 3.8: *The coupling between the pick-up loop and a dipole with a diameter of 2 μm and an x polarization with a varying diameter of the pick-up loop. The distance between the pick-up loop and the dipole is 10 μm. A bigger loop clearly gives a higher coupling, although the growth diminishes for bigger pick-up loops.*

sample so we have also chosen for a square loop to be able to compare the results of the easy MRFM with current ones.

In figure 3.8 the coupling is plotted for an increasing diameter of the pick-up loop. It clearly shows a diminishing growth. While the induced current in the pick-up loop is positively affected by the coupling, it is negatively affected for a longer pick-up loop. $I = \Phi/L$ shows that the current drops with a larger inductance, which happens for a bigger loop. Table 3.2 shows the calculated inductance and resulting current. The induced current is dependent on the amplitude of our resonator but is highest for a small pick-up loop.

Table 3.2: *Induced current in pick-up loop under the same circumstances as figure 3.8. The conductance is calculated for a square wire with 0.5 μm diameter and a relative permeability of 1.*

Size loop (μm)	5x5	6x6	7x7	8x8	9x9	10x10	11x11	12x12
$\Phi\left(\frac{\mu\Phi_0}{nm}\right)$	37.8	48.1	57.9	67.7	76.9	86.3	94.8	103.3
L (pH)	8.89	11.5	14.3	17.2	20.2	23.3	26.5	29.7
$I\left(\frac{kA}{nm}\right)$	8.80	8.65	8.37	8.14	7.87	7.66	7.40	7.19

As shown in figure 3.6 the coupling to the pick-up loop is highly dependent on the positioning of the cantilever with respect to the pick-up loop.

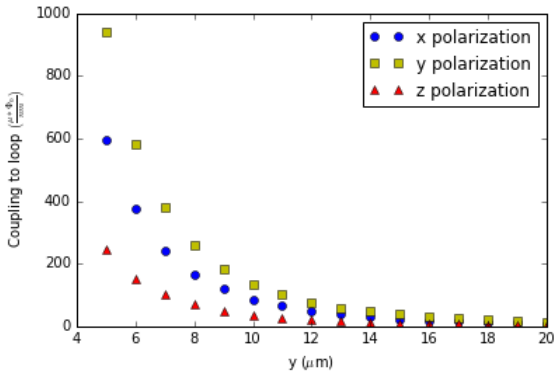

Figure 3.9: *The coupling between three polarizations of a 2 μm dipole and a square pick-up loop with a 10 μm diameter. We vary the distance between the pick-up loop and the cantilever on the y-axis, taking the value of the maximal coupling as in figure 3.6. The coupling is strongest for the y-polarization and weakest for the z-polarization.*

The precise position can be set in the final assembly of the Easy MRFM. For now the important thing is the maximal coupling. Figure 3.9 shows the maximal coupling for the x-, y-, and z-polarizations with a varying distance between the cantilever and loop over the y-axis. Higher coupling is achieved by putting the loop close to the cantilever. The best coupling is given for the y-polarization. Still it is only a factor 1.5 bigger than the x-orientation. In contrast to the coupling to the sample, the z-orientation would give the worst coupling to the pick-up loop.

The best set-up for the easy MRFM would have a magnet with a y-polarization as close to the cantilever as mechanically possible. We eventually chose to go with the polarization in the x direction, even though we would have a bigger coupling in y. This is because in our first test we wanted to replicate earlier results from our group which were measured with an x-polarization. By eventually using the y-polarization a factor 3 increase in the coupling could be achieved. However it is easier to increase the total signal by optimizing the coupling of the magnetic signals from the pickup loop to the SQUID, where currently about 99% of the signal is lost. In our group work is being done to significantly decrease the loss of signal to our SQUID and in theory a loss of only 50% has been predicted [13].

Chapter 4

Fitting procedure for high crosstalk data

In the Easy MRFM the pick-up loop and its transformer would be much closer to the piezo (and associated wires) that drives the cantilever. This could potentially cause a lot of crosstalk in our output signal. This transforms the signal in such a way that our current fitting procedures would not work well on the data. In this chapter we will describe a new method to extract the resonance frequency and quality factor from our data and show how it compares to our current methods.

4.1 Data representation

Our current measurements of MRFM consists of driving the piezo at a certain frequency causing the cantilever to oscillate. By sweeping through a frequency range with small steps we gather the amplitude and phase (ϕ) of our signal. When the resonance frequency of the cantilever is within the frequency range, the plotted amplitude should have a clear peak like in figure 4.1 and the plotted phase should have a clear phase shift of roughly 180 degrees like in figure 4.2. Both as predicted by the tranfer function derived in equation 2.4. By fitting the data it is thus relatively straightforward to get the resonance frequency as is explained in the theory section.

Crosstalk can occur when magnetic fields generated by currents in the wires of the cantilever piezo are picked up by the detection mechanism (SQUID, pick up loop, transformer, etc). Measurements with a lot of crosstalk will not always show a clear peak in the amplitude and a clear 180 degree shift in the phase. An example of a measurement with a signif-

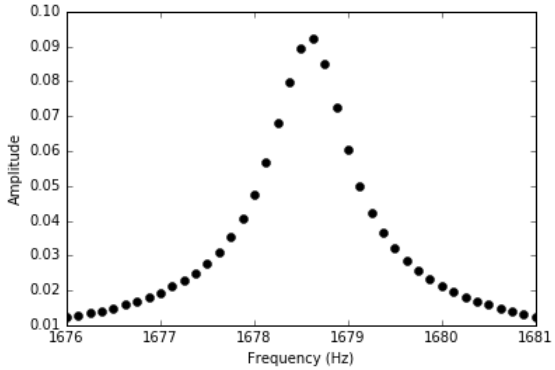

Figure 4.1: *The measured amplitude of our signal vs the frequency at which we drive the piezo. There is a clear peak around 1678 Hz, signifying that this could be the resonance frequency.*

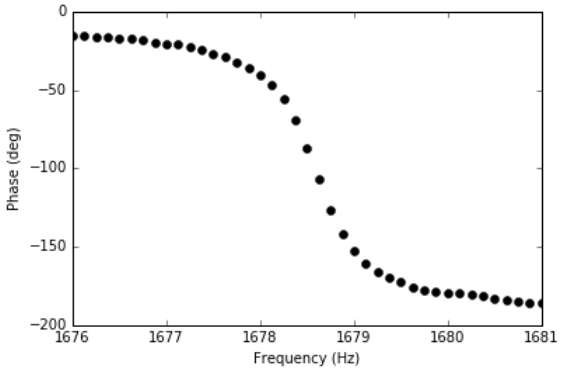

Figure 4.2: *The measured phase of our signal vs the frequency at which we drive the piezo. There is a clear shift in the phase of roughly 180 degrees around 1678 Hz, signifying that this could be the resonance frequency.*

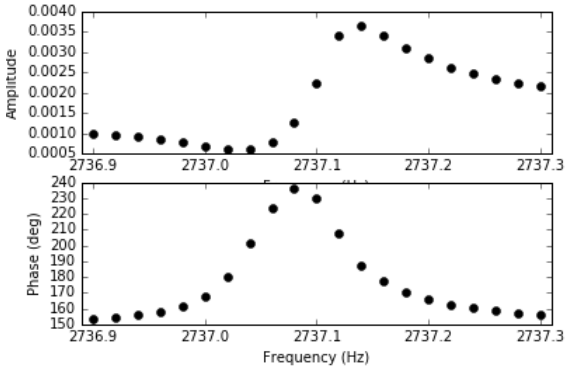

Figure 4.3: *The amplitude and the phase of a measurement of another cantilever with a lot of crosstalk. While it is clear something is happening around 2735.4Hz the plot does not show a clear peak in the amplitude and the phase plot does not show a clear shift.*

icant level of crosstalk is shown in figure 4.3. Due to the distorted shape of the peak, it is not possible to fit this data with a Lorentzian function without additional processing.

There is a way to display the data more clearly while preserving all the relevant information. If we take the amplitude of a measurement as R and the phase as ϕ we can compute $R * (cos(\phi) + i * sin(\phi))$ for every data point and plot it in the complex plane. In this representation measuring around the resonance frequency will result in a circle like the one shown in figure 4.4.

A good measurement starts in the origin and has the peak of the circle on the positive y-axis across from the origin. This peak has the maximum amplitude and the steepest slope for the phase which signal that the frequency at that measurement is the resonance frequency. Crosstalk in our measurement can cause a displacement and rotation of the circle. Still the resonance frequency is located at the peak across the reference point. Below we describe a new method based on the inverse mapping technique by Petersan and Anlage. [14]. The method utilizes the fact that the resonance frequency should be situated at the top of the circle and approximates the resonance frequency of an imaginary point placed there, shown as the red square in figure 4.4.

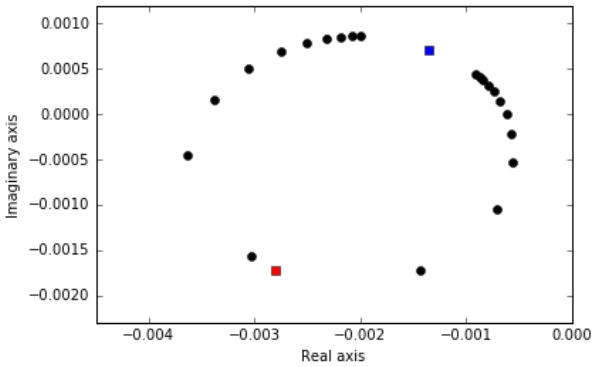

Figure 4.4: *The same data from 4.3 but then represented within the complex plane. The data shows a clear circle where we call the point between the first and the last datapoint, signified by the green square, the start of the circle and the red square the top of the circle. The resonance frequency can be calculated from a circle fit.*

4.2 Calculating the resonance frequency

The method below is based on the inverse mapping technique by Petersan and Anlage [14]. For a full explanation of the technique we refer to their paper but below we will try to explain the method in an intuitive manner.

The first step in the inverse mapping technique is making a fit of the circle. For a measurement with a potential large noise the best way to fit the circle is through a weighted least squares method. We first define a reference point (x_{ref}, y_{ref}) which is the point in between the first and the last datapoint. We then give each data point a weight according to its distance from the reference point, $W = [(x_{ref} - x_i)^2 + (Y_{ref} - y_i)^2)]$. From this fit we extrapolate the center and radius of the circle.

Inverse mapping uses three data points called f_1, f_2 and f_3 which are picked at random but should be close to the top of the circle (f_2) and approximately one bandwidth above (f_1) and below (f_3) (figure 4.5b). We first approximate f_1, f_2 and f_3 by rotating the reference point around the center of the circle by $\frac{1}{2}\pi, \pi$ and $\frac{3}{2}\pi$. We then randomly choose a point within an angle range of $\frac{1}{4}\pi$ from this approximation point with the center.

We can finally calculate the resonance frequency by using the complex frequency plane. We insert the frequencies of f_1-f_3 into the complex frequency plane as $i * f_i$, essentially placing them on the y-axis. We then use

Version of January 22, 2018– Created January 22, 2018 - 16:50

f_1-f_3 to find another point in this plane called the pole which is positioned at $if_0 - \frac{\Delta f_{Map}}{3}$.

We can calculate this pole using the fact that the angle between $f_{1/3}$, the origin and f_2 in the circular plot is equal to the angle between $f_{1/3}$, the pole and f_2 in the complex frequency plane (See figure 4.5). We then know that the position of the pole should be $if_0 - \frac{\Delta f_{Map}}{3}$ and thus the y position of the pole should equal the resonance frequency. We can also calculate the quality factor as it should equal $\frac{f_0}{\Delta f}$. When doing this procedure only once, we obtain a rough estimate of f_0 and Q due to the randomly picked location of f_1-f_3. However, when averaging this procedure over several iterations with new choices for f_1-f_3, we obtain a very precise and stable approximation of f_0 and Q.

4.3 Comparison with current methods

To check the accuracy of our new approach we have analyzed 40 different datasets, with and without crosstalk, and then compared the results with the fit parameters obtained from the traditional approach where we fit the amplitude data to a Lorentzian function. The result of this comparison can be seen in figure 4.6. The predicted resonance frequency overlaps almost perfectly with the current results and the the average distance is only 9.6 mHz. In general our new method gives a slightly higher estimate for the quality factor but almost all points still overlap. Only dataset 39 really differs from the predicted Q which can have multiple causes. Still with an average difference of only 385 we can conclude that the new method nicely estimates F0 and Q.

We also gathered some datasets with a lot of crosstalk. Figure 4.7 shows the comparison of these datasets. Although the predicted resonance frequencies have a large standard deviation the predicted results again overlap almost perfectly with an average difference of only $7.6 * 10^{-3}$. While the quality factor seems to also compare quite nicely dataset 1 shows a clear discrepancy between the results.

The cause of the big difference between the obtained quality factor of dataset 1 for the two approaches is not immediately apparent. Figure 4.8 takes a more in depth look into the fit of our new procedure for dataset 1. It shows the fit of the circle and the chosen f1, f2 and f3 for one iteration in the program. It is likely that the lack of points around the resonance frequency

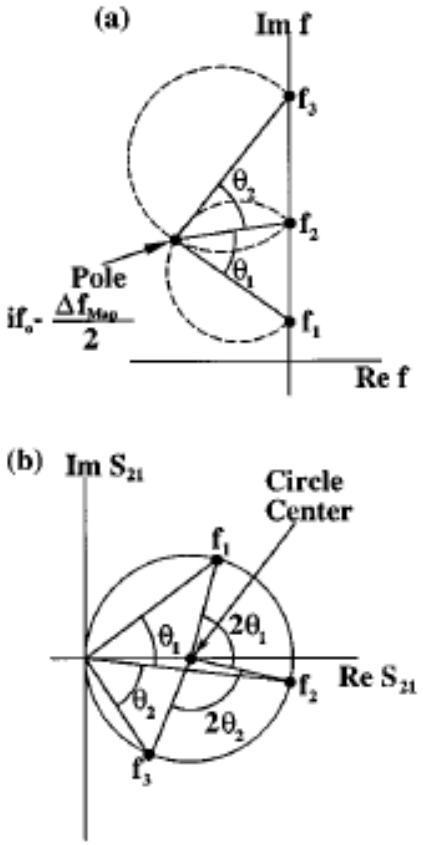

Figure 4.5: *Two pictures showing the inverse mapping technique A) The mapping of the three points into the complex frequency plane. Because the angles $\theta_{1/2}$ are preserverd it is possible to calculate the position of the pole and thus find the resonance frequency. B) From the center of the circle that is calculated by the fit of our data, and the three randomly chosen points, we can determine the angles $\theta_{1/2}$. [14]*

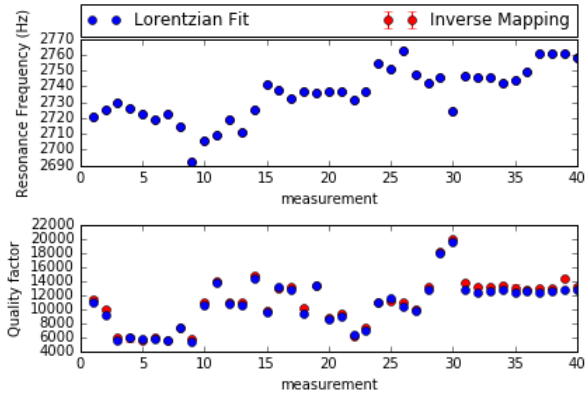

Figure 4.6: *A comparison between current fitting procedures and the prediction of our new method for the resonance frequency and the quality factor.*

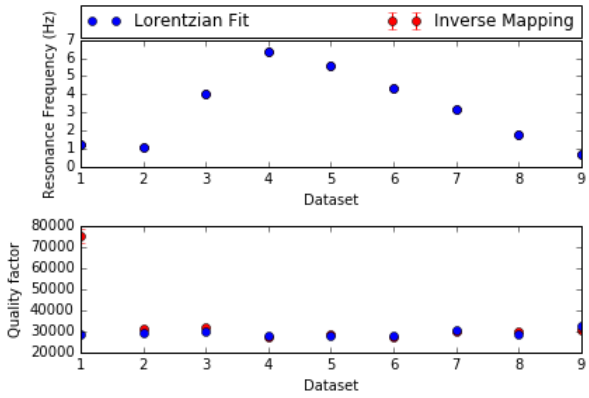

Figure 4.7: *A comparison between datasets with a lot of crosstalk. The current results are made through rotating and displacing the polar plots by hand back to their origin. These new plots are the fitted.*

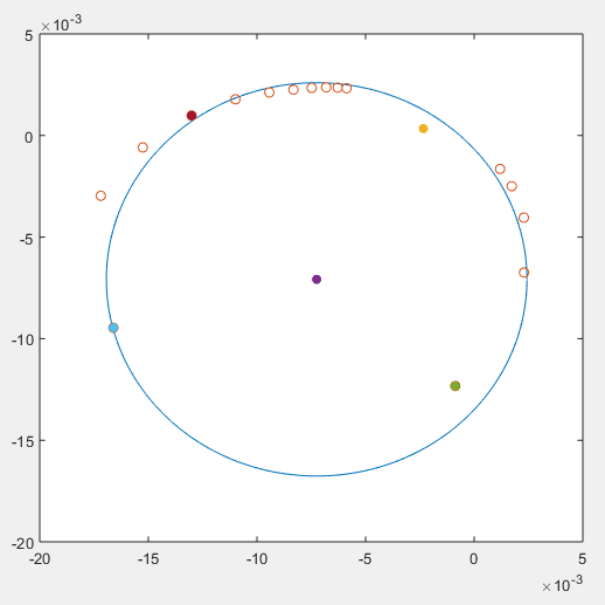

Figure 4.8: *an in depth look at cross talk dataset 1. The points shown in the picture are the center, the reference point and F1, F2 and F3.*

causes the error in the predicted quality factor. We therefore conclude that the faulty fit was not due to the procedure, but the low quality of the data.

If we discard dataset 1 the average difference in the quality factors is 1130. It is expected that the average difference between quality factors is higher for the data with crosstalk. This is because the original fitting procedure is done by eye which should give the results a bigger error margin. All in all, our new method seems to be a nice replacement for our current one. While both methods have comparable results, for measurements with a lot of crosstalk it provides a fully automated and less error prone procedure.

Chapter 5

A new cantilever

The degree of precision in your MRFM measurements strongly depend on the kind of cantilever that is used. Because a bigger Q-factor means a better defined peak and a slower damping, smaller forces will have a measurable effect on the cantilever. A higher Q-factor will thus give us the ability to measure on a smaller scale and is of vital importance in the improvement of MRFM.

Our current cantilevers are made of single crystal silicon and have a length, width and thickness of respectively 145 μm, 5 μm and 100 nm. In an optimal environment of a vacuum with temperatures of a few Kelvin they can reach a Q-factor of $5 * 10^5$ while maintaining a resonance frequency in the range of a few kHz.

This chapter is about our hunt for new, improved cantilevers. We start with a description of the new cantilevers and of their production process after which we will characterize and compare them with our current cantilevers.

5.1 Preparing silicon nitride cantilevers for MRFM

Recent advances in the field of resonators have shown Silicon Nitride as a very promising material for cantilevers with Yuan et al. reaching Q-factors exceeding 10^8 for high stress cantilevers at milikelvin temperatures [15]. This motivated us to buy a batch of ultra-soft silicon nitride probes from the company Nunano [16] to see if we could use them to improve our current experiments. These probes have a length of 130 μm, a width of 1 μm and a 100 nm thickness. The silicon nitride used has a Young's modulus of 210 GPa and a density of 3100 kgm-3. This gives them a stiffness of

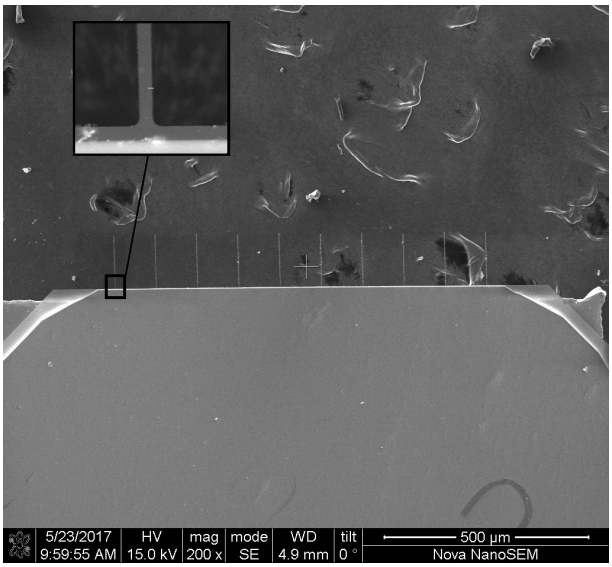

Figure 5.1: *A picture made inside a Scanning Tunneling Microscope showing a Nunano chip consisting of 10 probes. For the eventual measurements 9 probes are manually removed from the chip.*

25 μN/m and a bare resonance frequency of roughly 8 kHz. A magnetic particle of a few μm in diameter would bring the resonance frequency into our preferred regime of 2 - 4 kHz.

A chip contains ten probes on one side (figure 5.1). Because in our experiments we only use one cantilever we decided to remove the probes that we would not use. This prevents us aligning the wrong probe in our set-up.

It is worth noting that the first shipment we received from Nunano contained contaminated probes as can be seen in figure 5.2. The problem was probably caused in their critical point drier which was often used for biological samples. By switching to another critical point drier which was primarily used for semiconductor/MEMS devices their problem was solved and their second shipment had no problems with any contaminations.

5.1.1 Producing a magnetic field

To be useful in MRFM these probes need to produce a magnetic field. to achieve this we attach a particle from a high performance anisotropic powder to the cantilever. This powder, MQA-38-14, is developed by Magnequench Technology center. We place the cantilever on a nanomanipula-

Version of January 22, 2018– Created January 22, 2018 - 16:50

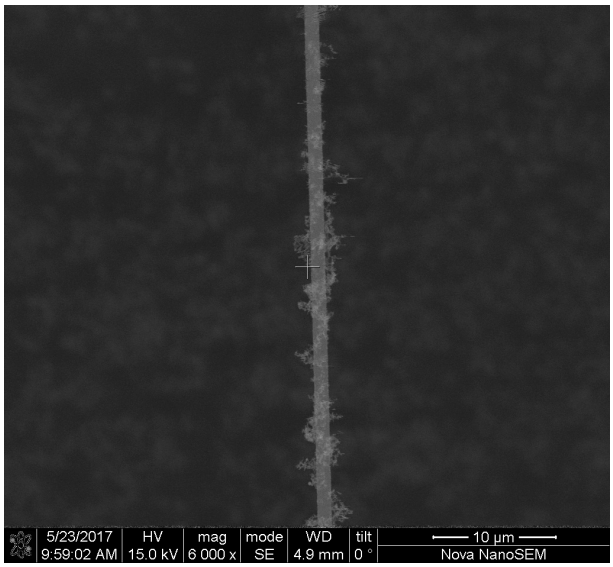

Figure 5.2: *A probe from the first shipment of Nunano. The contamination around the cantilever is clearly visible. Nunano changed their manufacturing process and a new shipment was free of any contaminations.*

tor which allows us to align the end of the cantilever on a magnetic particle of choice.

Figure 5.3 shows us the nanomanipulator and its various parts. We can roughly divide it in two sections, one side holding a film with particles and one holding the cantilever. The film consists of carbon tape on a small copper sheet. The particles stick on the carbon tape and the whole film is placed under a small clip on the nanomanipulator. We control the part of the nanomanipulator holding the film using attocubes which have a step size of roughly 0.5 μm. The chip with the cantilever is fixed in the nanomanipulator with a spring. We control it using three piezoelectric elements with a range of approximately 5 μm[17].

The nanomanipulator is placed inside a Scanning Electron Microscope (SEM) which shows us the particle and cantilever in real time (figure 5.4. First a suitable particle with the right diameter has to be chosen. Aligning this particle with the end of the cantilever is no easy task. The new Si3N4 cantilevers are extremely flexible and sensitive to charging through the bombardment of electrons in the SEM. With the wrong settings it is even possible to bend the cantilever a full 180 degrees, sticking it to its own chip. To prevent this we reduce the spotsize and decrease the voltage for the beam. By doing this we decrease the amount of electrons that reach the cantilever as much as possible while keeping a clear image. This

Version of January 22, 2018– Created January 22, 2018 - 16:50

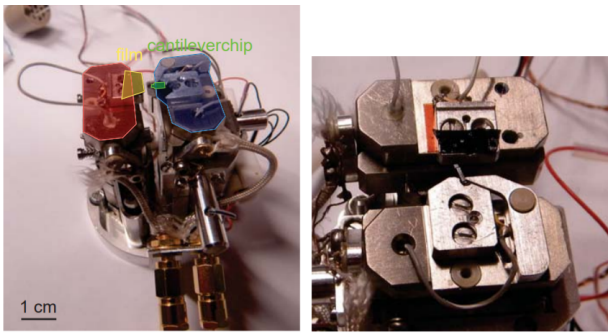

Figure 5.3: *A picture from the nanomanipulator[18] which we use to attach magnetic particles on the film (yellow) to a cantilever (green). The red part is the filmholder which can be moved using attocubes, the blue part is the cantileverholder which moves through a piezoelectric element.*

increased sensitivity to electrostatic charges compared to our previous Si cantilevers is probably a result of the material used. While the resistivity of single crystal silicon is roughly $10^5\ \Omega * m$ the resistivity of silicon nitride is roughly $10^{14}\ \Omega * m$ [19].

When contact is achieved between the cantilever and the chosen particle we use the Electron Beam Induced Deposition (EBID) procedure to permanently attach them to each other. After the particle is attached we place the cantilever in a magnetic field of roughly 5 T, resulting in a permanent magnetization of the particle of roughly 1.2 - 1.3 T [20]. All produced cantilevers for this theses have been magnetized in the direction in which the cantilever resonates.

5.2 Characterization and comparison

We need to know the behaviour of the new cantilevers in the environment of current measurements to see if they can substitute current cantilevers. For this we used two Nunano cantilevers as described in chapter 5.1 that we call cantilever 1 and cantilever 2, differing only in the size of their magnetic particles. The particle on cantilever 1 has a radius of 2.96 μm and the particle on cantilever 2 has a radius of 3.74 μm.

To make comparative measurements it is easiest to replicate the conditions of current MRFM measurements. This is done by placing the cantilever in a box, directly above a SQUID (figure 5.5). We then mount the SQUID box at the cold end of a dipstick intended for use in liquid helium. The vacuum cone of the dipstick is covered with Nb foil to act as a super-

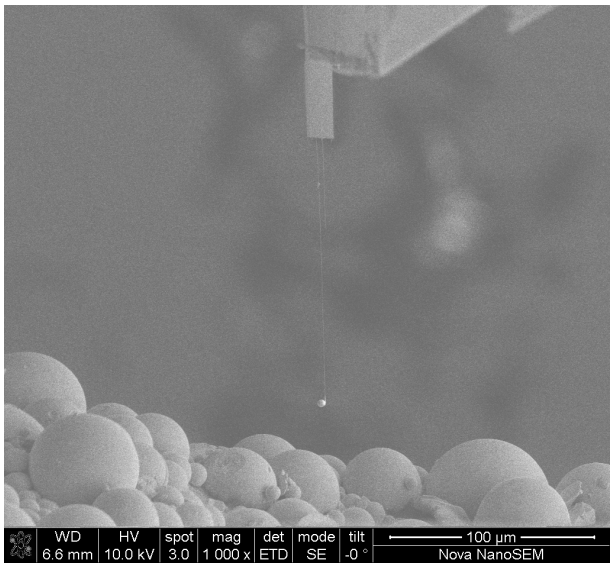

Figure 5.4: *The cantilever with a particle of a few nm close to the surface of the film holding the magnetic particles. Using nanomanipulation we contact the cantilever to a chosen particle of the right diameter after which we are able to fasten them to each other.*

conducting shielding against external magnetic noise.

In these measurements we managed to create a vacuum of roughly $10^{-}3$ mbar at a temperature of roughly 4.2 kelvin. The remaining pressure is probably caused by helium leaking inside the dipstick while the temperature was measured using a calibrated RuO2 10kOhm thermometer mounted near the SQUID box. We can now make measurements in a low temperature vacuum using the SQUID which is also done in real MRFM measurements. Although our current MRFM measurements have a much better vacuum which explains their higher measured Q-factors.

For our experiments the most important property of a cantilever is the behaviour of its Q-factor. With cantilever 1 we made some measurements to check the stability of the cantilever. The same measurement was done 8 times over a time period of roughly 16 minutes. Figure 5.6 shows that the quality factor of the cantilever decreases over time. The decrease could be attributed to leftover gasses freezing to the cantilever. A good indication that this is really happening is the same decrease measured in the resonance frequency.

With cantilever 2 we focussed on the behaviour of the Q factor against a varying pressure inside the protective casing. Figure 5.7 shows the re-

Version of January 22, 2018– Created January 22, 2018 - 16:50

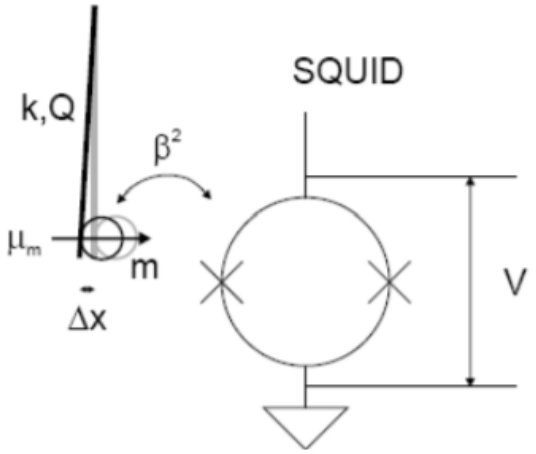

Figure 5.5: *A schematic explaining our measurements. The cantilever is placed above a SQUID which creates a current because of the varying magnetic field from the resonating dipole. [21]*

sults plus the same measurement for one of our currently used IBM silicon cantilevers described at the start of this chapter. As a reference the results of the measurements of cantilever 1 are also plotted. It is clear that the decrease over time is insignificant to general fluctuations. Cantilever 2 shows a clear relation between the pressure inside the casing and the Q factor. In general the Q factor of the new cantilevers seems to be higher than that of the IBM cantilever while also appearing more stable.

For now we conclude that the Nunano cantilevers could be a reasonable replacement for the current IBM cantilevers. In comparative circumstances the measured Q-factor appears more stable and generally higher than current cantilevers. We did show that the Q-factor is pressure dependent, which if we combine this with the fact that the frontal surface of the new cantilevers is 5 times smaller, makes it hard to predict their eventual Q-factors in real MRFM measurements. However their intrinsic damping should not be worse than in our current cantilevers.

Although the quality factor seem to degrade over time this should not be attributed to the intrinsic properties of the new cantilevers, as it seems likely that this is caused by a leak in the dipstick vacuum. In general, the intrinsic damping of the cantilevers seems to be competitive to the traditional IBM cantilevers. The biggest downside of the new cantilevers compared to the IBM type is their higher resistivity which increases the complexity of attaching our magnetic particles in the SEM due to charging, but could also increase electrostatic interactions between the tip and the

Version of January 22, 2018– Created January 22, 2018 - 16:50

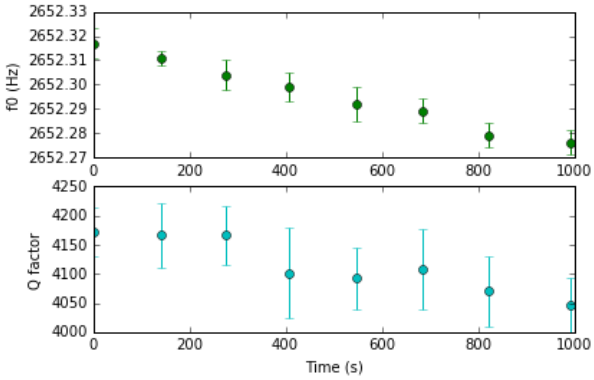

Figure 5.6: *Both the reference frequency and the Q-factor of our cantilever seem to decrease over time. This is possibly caused by ice forming on the cantilever through a leak in the vacuum.*

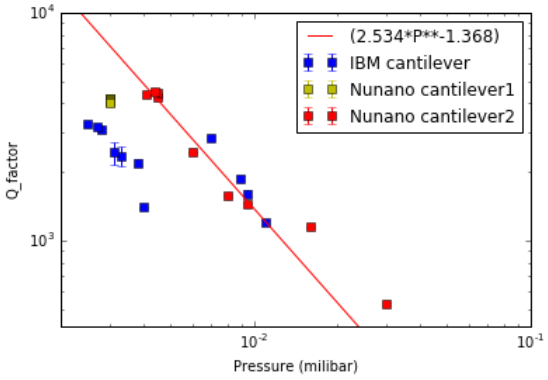

Figure 5.7: *The Q-factor plotted against the pressure of a new Nunano cantilever and an old IBM cantilever. The results from figure 5.6 are also plotted as a reference. The results from Nunano cantilever2 have been fitted, showing an relation between the pressure and the Q-factor.*

sample in the MRFM experiments.

Chapter 6

Conclusion & Discussion

We have done theoretical calculations for the configuration and design of a new set-up called the Easy MRFM, in which the pick-up loop would be placed next to the cantilever. According to our predictions this set-up should be feasible and it is now in production. In chapter 3, we have found that in terms of signal the optimal setup consists of a y-polarized cantilever. However, we have adviced to start with an x-polarized cantilever as this closely resembles the convential MRFM in our group. This would make the eventual comparisons between results of the Easy MRFM and current measurements easier to interpret.

We further anticipated that this new set-up would increase the crosstalk in our measurements. Because current fitting procedures do not handle crosstalk data well, we implemented a new method described in chapter 4. This new method gives comparable results with current methods but is fully automated and less error prone. This new method is currently being integrated in our measurement programs by my successor Daniel Opdam.

We have also made comparative measurements for a new type of cantilever. We mostly focussed on the behaviour of its resonance frequency and quality factor. In these parameters the new cantilevers appear equal or even slightly better than current cantilevers. They seemed to show some degradation in time in their quality factor and resonance frequency but we could not rule out other factors causing this. We could conclude that this possible degradation is negligible compared to their dependence on the present vacuum. The biggest downside is their high sensitivity to electrostatic forces making them difficult to handle while preparing them for MRFM measurements. Further research should also conclude if this would have an effect on measurements with real samples.

Bibliography

[1] D. Rugar, C. S. Yannoni, and J. A. Sidles, *Mechanical detection of magnetic resonance*, Nature **360**, 563 (1992).

[2] C. L. Degen, M. Poggio, H. J. Mamin, C. T. Rettner, and D. Rugar, *Nanoscale magnetic resonance imaging*, Proceedings of the National Academy of Sciences **106**, 1313 (2009).

[3] J. J. T. Wagenaar, *Magnetic resonance force microscopy for condensed matter*, 2017.

[4] J. P. Cleveland, S. Manne, D. Bocek, and P. K. Hansma, *A nondestructive method for determining the spring constant of cantilevers for scanning force microscopy*, Review of Scientific Instruments **64**, 403 (1993).

[5] R. J. Wood, E. Steltz, and R. S. Fearing, *Nonlinear Performance Limits for High Energy Density Piezoelectric Bending Actuators*, in *Proceedings of the 2005 IEEE International Conference on Robotics and Automation*, pages 3633–3640, 2005.

[6] M. Mukhopadhyay, *Vibrations, Dynamics and Structural Systems 2nd edition*, CRC Press, 2000, Google-Books-ID: SeC8hvI2QywC.

[7] C. Sundararajan, *Compendium of Formulas for the Structural Vibration Frequency Analysis of Beams*.

[8] J. J. T. Wagenaar, A. M. J. d. Haan, R. J. Donkersloot, F. Marsman, M. de Wit, L. Bossoni, and T. H. Oosterkamp, *A method for mechanical generation of radio frequency fields in nuclear magnetic resonance force microscopy*, Physical Review Applied **7** (2017), arXiv: 1609.05685.

[9] R. Donkersloot, *The potential of higher eigenmodes in magnetic resonance force microscopy*, 2016.

[10] *Delft Circuits (www.delft-circuits.com)*.

[11] J. M. de Voogd, J. J. T. Wagenaar, and T. H. Oosterkamp, *Dissipation and resonance frequency shift of a resonator magnetically coupled to a semi-classical spin*, arXiv:1508.07972 [cond-mat, physics:quant-ph] (2015), arXiv: 1508.07972.

[12] W. C. Young and R. G. Budynas, *Roark's Formulas for Stress and Strain*, McGraw Hill Professional, 2001, Google-Books-ID: pummClLoFXEC.

[13] J. M. de Voogd, *Magnetic resonance force microscopy and the spin bath, unpublished Doctoral thesis*.

[14] P. J. Petersan and S. M. Anlage, *Measurement of resonant frequency and quality factor of microwave resonators: Comparison of methods*, Journal of Applied Physics **84**, 3392 (1998).

[15] M. Yuan, M. A. Cohen, and G. A. Steele, *Silicon nitride membrane resonators at millikelvin temperatures with quality factors exceeding 108*, Applied Physics Letters **107**, 263501 (2015).

[16] *NuNano Ultra-soft Probes (www.nunano.com)*.

[17] E. C. Heeres and F. d. W. e. Natuurwetenschappen, *Manipulating carbon nanotubes Towards the application as novel field emission sources*, 2014.

[18] H. C. Overweg, *Smaller magnets for larger field gradients in Magnetic Resonance Force Microscopy*.

[19] V. Semiconductor, *The General Properties of Si, Ge, SiGe, SiO2 and Si3N4*.

[20] H. C. Overweg, A. M. J. den Haan, H. J. Eerkens, P. F. A. Alkemade, A. L. La Rooij, R. J. C. Spreeuw, L. Bossoni, and T. H. Oosterkamp, *Probing the magnetic moment of FePt micromagnets prepared by focused ion beam milling*, Applied Physics Letters **107**, 072402 (2015).

[21] O. Usenko, A. Vinante, G. Wijts, and T. H. Oosterkamp, *A SQUID based read-out of sub-attoNewton force sensor operating at millikelvin temperatures*, arXiv:1007.1572 [cond-mat, physics:physics] (2010), arXiv: 1007.1572.